The Astrophysical Journal, 690:734–742, 2009 January 1 doi:10.1088/0004-637X/690/1/734

SPATIAL CORRELATION OF SOLAR WIND FLUCTUATIONS AND THEIR SOLAR CYCLE DEPENDENCE

R. T. Wicks[1], S. C. Chapman[1], and R. O. Dendy[1,2]
[1] Centre for Fusion, Space and Astrophysics, Department of Physics, University of Warwick, Coventry, CV4 7AL, UK; R.Wicks@warwick.ac.uk
[2] UKAEA Culham Division, Culham Science Centre, Abingdon, Oxfordshire, OX14 3DB, UK
Received 2008 June 30; accepted 2008 September 5; published 2008 December 1

ABSTRACT

We investigate the spatial correlation properties of the solar wind in the ecliptic at 1 AU using simultaneous in situ observations by the Advanced Composition Explorer and *Wind* spacecraft. We present the first direct study of the spatial correlation length scale λ of fluctuations in the solar wind ion density ρ, and find it to be smaller than that of the magnetic field. We find that there is the same statistically significant increase in λ by a factor $\approx$2 from solar minimum to solar maximum for both density and magnetic field magnitude, in contrast to the components of the field, whose λ shows no discernible solar cycle variation. This is suggestive of long-range correlation in ρ and $|B|$ which is of direct coronal origin, in contrast to that found in the **B** components, which is more strongly dominated by in situ evolving turbulence. The distinct correlation lengths of the density and magnetic field, and their solar cycle variation, thus provide new quantitative insights into coronal processes and their mapping out into the solar wind. These results also provide quantitative input for models of cosmic ray propagation within the heliosphere.

Key words: cosmic rays – solar wind – turbulence

Online-only material: color figures

1. INTRODUCTION

In situ solar wind plasma observations over the last 30 years show that its local properties at 1 AU are modulated by the solar cycle (e.g., Hapgood et al. 1991) and that this has an impact on the terrestrial magnetosphere and ionosphere (e.g., Johnson et al. 2005). There is evidence for more mixing of fast and slow solar wind plasma at solar maximum (e.g., Bame et al. 1976) and changing magnetic field complexity over the cycle (Kiyani et al. 2007; Hnat et al. 2007). One method for quantifying the effect of solar activity on the solar wind is to determine the correlation length scale λ of fluctuations measured in situ. Understanding the spatial correlation of the fluctuations of the flow is important for attempts to interpret solar wind properties in terms of the interplay between locally evolving turbulence (e.g., Goldstein et al. 1995; Pommois et al. 2001) and the coronal driver. Both turbulence (Hill et al. 2002) and large-scale coherent structures (Mason et al. 2008) have consequences for cosmic ray propagation within the heliosphere, which shows solar cycle dependence (e.g., Milano et al. 2004). Characterization of solar wind fluctuations is an important element of models for the propagation of particles in the heliosphere in this context (e.g., Parhi et al. 2002; Qin et al. 2006; Ruffolo et al. 2003; Webber et al. 2003; Zank et al. 1998).

There are two complementary approaches to calculating λ: (1) using the Taylor hypothesis (Taylor 1938) with single-spacecraft timeseries, and (2) using simultaneous data from multiple spacecraft as done here (see also Matthaeus et al. 2005; Osman et al. 2007). The first approach has been very successful at predicting large-scale, slowly varying (measured on a timescale of hours) features of the solar wind and their propagation (e.g., Weimer et al. 2003; Ridley 2000). Using multiple spacecraft gives a correlation measurement over the separation distance of the spacecraft (Matthaeus et al. 2005; Osman et al. 2007) that is instantaneous. We use the *Advanced Composition Explorer* (*ACE*) and *Wind* spacecraft in our study, providing a range of spatial separations in the Geocentric Solar Ecliptic (GSE; Hapgood 1992) $\hat{x}$ direction from 3 to 160 R_E (one Earth radius $R_E = 6378.1$ km; we use GSE coordinates (Hapgood 1992) throughout).

The inertial range of solar wind turbulence (e.g., Bruno et al. 2006; Goldstein et al. 1995) typically spans timescales from under a minute up to a few hours, where we can anticipate both spatial and temporal fluctuations. For a typical solar wind speed of 550 km s^{-1}, a structure in the solar wind will need to vary on a timescale much longer than 20 minutes in order to propagate essentially unchanged between *Wind* and *ACE*, given a typical spacecraft separation of $100R_E$. The instantaneous measure of spatial correlation that is provided by simultaneous *Wind* and *ACE* observations thus probes spatiotemporal fluctuations typical of inertial range turbulence in the solar wind.

In this study, we use simultaneous observations by *ACE* and *Wind* of both magnetic field **B** and ion density ρ to directly quantify the spatial correlation. Previously, for the magnetic field **B**, these observations have been used to show anisotropy in the solar wind (Milano et al. 2004) and to measure the Taylor microscale (Matthaeus et al. 2005). Here we determine the correlation properties of ρ for the first time, and find that there is a difference in the spatial correlation properties of ρ and **B** (both components and magnitude), and that λ for ρ and for $|B|$ increases by a factor of 2 from solar minimum to solar maximum.

We also test the linear correlation measurements against other parameters that might affect the correlation properties of the flow. In particular, we show that neither the solar wind speed nor the orientation of the spacecraft in the solar wind straightforwardly order the observed correlation length scale, which shows high variability. Finally we use a nonlinear measure of correlation, mutual information (MI), to confirm our results hold without the assumption of linearity.

2. ANALYSIS

We use the linear cross-covariance to provide a measure of correlation between two signals A and B, defined by

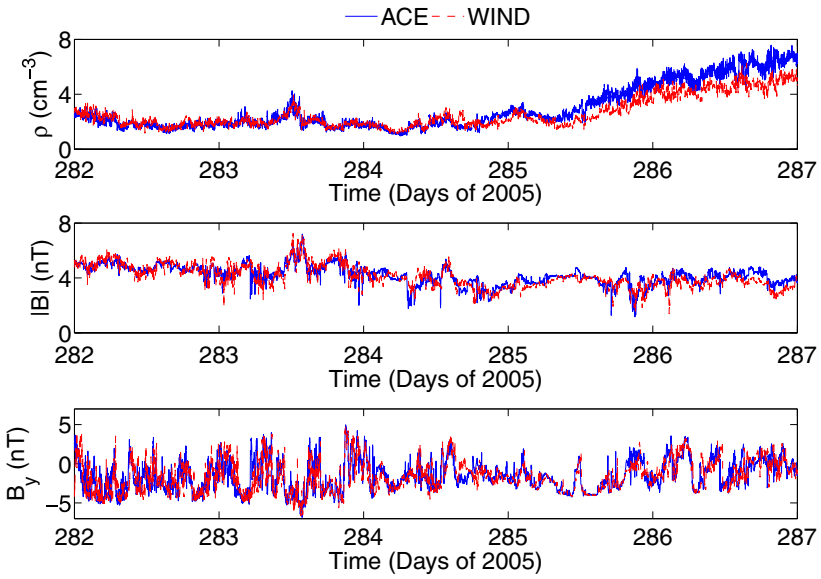

Figure 1. Typical 5 day period of solar wind observations from the *ACE* (solid blue line) and *Wind* (dashed red line) spacecraft. The top panel shows the ion density, ρ (cm^{-3}), the middle panel the magnetic field magnitude, $|B|$ (nT), and the bottom panel the $\hat{y}$ component of the magnetic field, B_y (nT).

$$C(A, B) = \frac{E[(A - \overline{A})(B - \overline{B})]}{\sqrt{E[(A - \overline{A})^2]E[(B - \overline{B})^2]}}, \quad (1)$$

where $E[\cdots]$ denotes the mathematical expectation value and $\overline{A} = E[A]$. A typical period of data from solar minimum is shown in Figure 1 which plots 5 days of observations of ion density, magnetic field magnitude, and the $\hat{y}$ GSE component of **B** from 2005.

Since we anticipate that the solar cycle will affect the spatial correlation in the solar wind, we take data from periods as near to solar minimum as possible (that is, in 1998, 2005, and 2006) and from solar maximum in 2000. In 1998, *Wind* was returning toward Earth from the Sun–Earth libration point while *ACE* orbited the libration point; in 2005 and 2006, both *ACE* and *Wind* orbited the libration point. Seventeen periods of data were chosen with different spacecraft separations, and the typical length of a period is 3 days, giving a total of 48 days of data. At solar maximum in 2000, *Wind* orbited the Earth and, therefore, only short periods when the spacecraft is suitably far from the magnetopause and bow shock could be used. Four such periods were used, giving a total of 15 days of data. Two-minute cadence data were used for all variables.

To compute the cross-correlation (1) from the data, it is necessary to define a window length τ, over which we compute signal expectation values. By moving this window through the data one step at a time, and recalculating statistical properties at each step, an ensemble average of these properties can be constructed.

We use two different lengths τ for our measurement window to optimize for two distinct timescales observed in the power spectrum (e.g., Nicol et al. 2008). We choose $\tau_L = 960$ minutes to include the large-scale structures, and $\tau_S = 200$ minutes to focus on the inertial range of turbulence in the solar wind. A shorter window cannot be used because the data in the window then become too short for a reliable correlation estimate to be made.

The linear correlation coefficient (1) is calculated for windows τ_S and τ_L as they are moved along the data. A value for linear correlation coefficient is thus obtained every 2 minutes for each window length, and 24 hr averages are then calculated and plotted against separation in Figures 2–4. Figure 5 and Table 1 summarize the results with errors. Figure 6 shows the results using the shorter window τ_S for $|B|$ and ρ, and compares them to the longer window τ_L.

Table 1
Values of Correlation Length λ, with 95% Confidence Bounds, in Earth Radii ($R_E = 6378$ km)[a]

Variable	Correlation Coefficient			
	$\lambda_{\min}$	R^2	$\lambda_{\max}$	R^2
$\|B\|$	118^{+21}_{-15}	0.30	274^{+104}_{-59}	0.49
ρ	75^{+11}_{-9}	0.57	167^{+78}_{-40}	0.20
B_x	123^{+25}_{-18}	0.05	194^{+84}_{-45}	0.20
B_y	144^{+16}_{-18}	0.36	169^{+40}_{-27}	0.55
B_z	125^{+66}_{-31}	0.50	169^{+34}_{-24}	0.40

Notes. Results here are estimated using the long window τ_L during solar minimum (1998, 2005, 2006) and solar maximum (2000). The R^2 values of each fit are provided to give an indication of the scatter in the data and thus the reliability of each resulting value of λ.
[a] Calculated by least-squares fitting of exponentials to the 24 hr mean linear correlation coefficient.

All of these results show a large degree of scatter, so we will analyze in more detail the distribution of measured correlation lengths in Figure 8, showing that the difference between maximum and minimum is measurable. In Figure 9, we plot 24 hr averages of cross-correlation against the 24 hr mean solar wind speed. Figure 10 shows the effect of the spacecraft orientation on the results.

3. DISCUSSION

Figure 2 plots linear correlation versus spacecraft separation for ρ, $|B|$, and **B** components at solar minimum using τ_L. We see that although there is substantial scatter, the correlations estimated for $|B|$ are systematically higher than those for ρ, whereas the $\hat{y}$ and $\hat{z}$ components of **B** have no systematic difference from each other. Figure 2 indicates, and Table 1

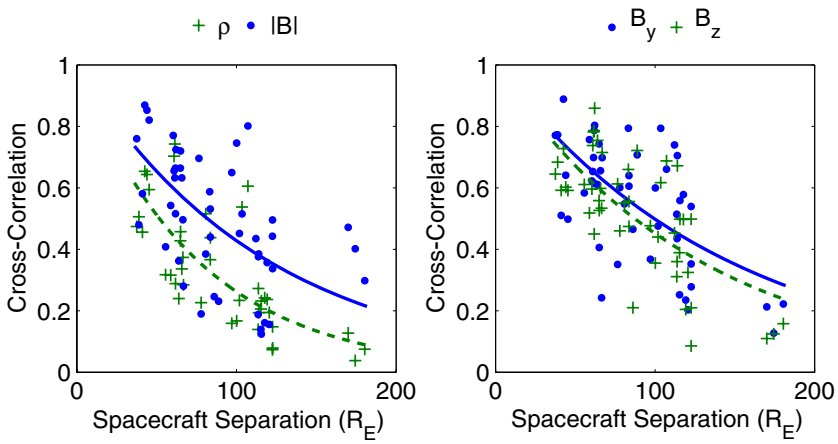

Figure 2. Linear correlation for $\tau_L = 960$ minutes at solar minimum, 24 hr averages plotted here vs. spacecraft separation. Density ρ ((+) and dashed line) is compared to magnetic field magnitude $|B|$ ((•) and solid line) in the left-hand panel. In the right-hand panel, the $\hat{y}$ and the $\hat{z}$ components (GSE) of **B** are compared. The lines are inverse exponential fits to the data.

(A color version of this figure is available in the online journal.)

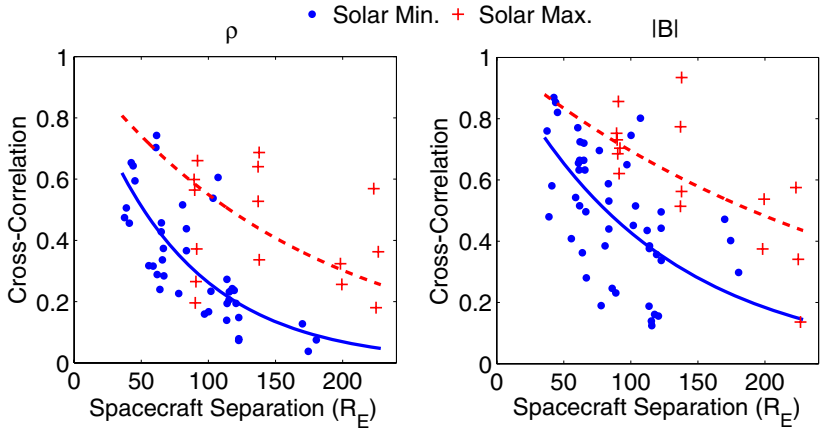

Figure 3. 24 hr mean linear correlation coefficients, between *ACE* and *Wind* $|B|$ and ρ for window length $\tau_L = 960$ minutes, for selected periods in 1998, 2005, and 2006 (solar minimum: (•) and solid line) and 2000 (solar maximum: (+) and dashed line). The lines are inverse exponential fits to the data.

(A color version of this figure is available in the online journal.)

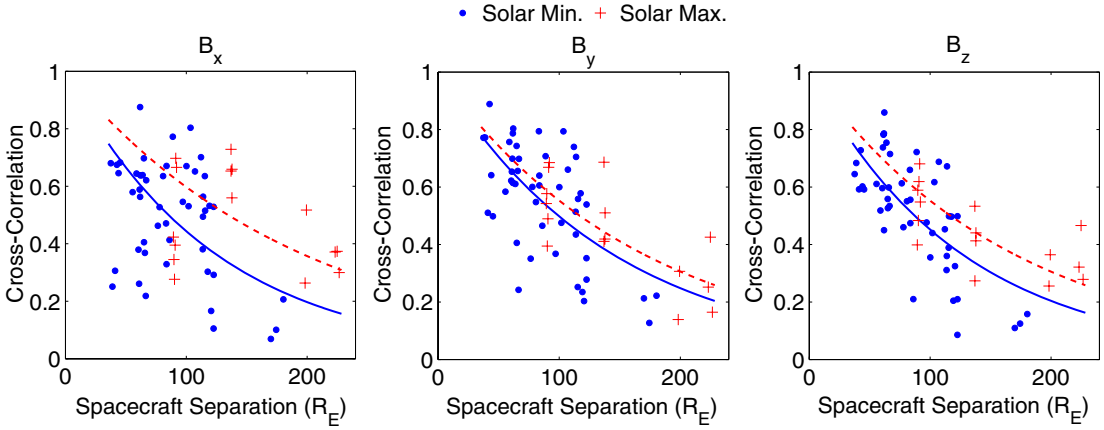

Figure 4. 24 hr mean correlation coefficients, between *ACE* and *Wind* B_x, B_y, and B_z using window length $\tau_L = 960$ minutes, for selected periods in 1998, 2005, and 2006 (solar minimum: (•) and solid line) and 2000 (solar maximum: (+) and dashed line). The lines are inverse exponential fits to the data.

(A color version of this figure is available in the online journal.)

confirms, that, at solar minimum, B_y and B_z are closer to $|B|$ than ρ.

We anticipate the spatial variation of linear correlation coefficient to be of exponential form (Matthaeus et al. 2005). Following Matthaeus et al. (2005) we therefore fit an exponential function $y = a\exp(-S/\lambda)$ to the data using nonlinear least squares, where y is the measure of correlation of the variable under consideration ($|B|$, B_x, B_y, B_z, or ρ) and S is the spacecraft

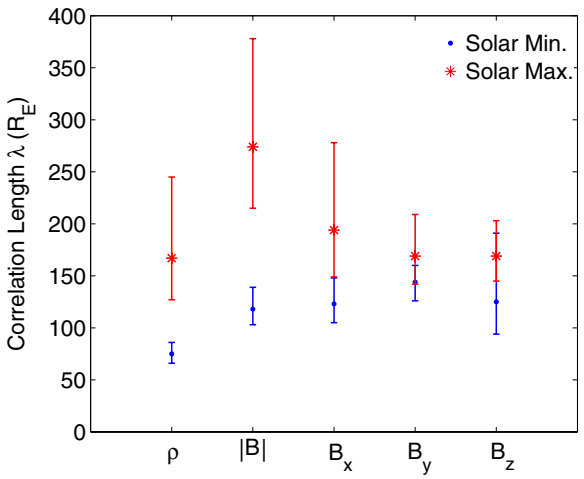

Figure 5. Correlation lengths λ estimated using window τ_L, calculated between *ACE* and *Wind* measurements using linear cross-correlation at solar minimum in 1998, 2005, and 2006 (•) and solar maximum (∗) in 2000 with the corresponding error bars as in Table 1.

(A color version of this figure is available in the online journal.)

separation with $a = 1$. The calculated values of λ are shown in Table 1 and Figure 5. The uncertainty on the correlation length is quantified by the 95% confidence bound of the nonlinear least-squares fit, and by the R^2 value for the fit:

$$R^2 = 1 - \frac{\Sigma_{i=1}^{n}(y_i - f_i)^2}{\Sigma_{i=1}^{n}(y_i - \overline{y})^2}, \quad (2)$$

where f_i is the fit, y_i are the data, and $\overline{y}$ is the mean of the data (Moore & McCabe 2006). This value characterizes how successful the fit is in explaining the variation of the data. A value of 1 indicates a perfect fit and a value close to 0 indicates a poor fit. We expect low values of R^2 because the data are very scattered. Values lower than 0.3 imply that the fit is unreliable. Further analysis of the scatter and the reliability of the results continues below and in Figure 8.

We now consider variation with solar cycle. Figure 3 plots linear correlation coefficient against spacecraft separation for $|B|$ and ρ. It shows that the cross-correlation yields higher spatial correlation in both ρ and $|B|$ at solar maximum than at solar minimum. To quantify this, we again fit an exponential of the form $y = a\exp(-S/\lambda)$, with $a = 1$. The calculated values of correlation length λ are shown in Table 1. We see that the correlation length estimated at solar minimum is systematically shorter than that at maximum.

These values are consistent with previous single- and multiple-spacecraft measurements of correlation lengths for magnetic field fluctuations in the solar wind; for example, previous multispacecraft studies with *Wind*, *ACE*, and CLUSTER (Matthaeus et al. 2005) give a value of $\lambda \approx 1.3 \times 10^{11}$ cm $\approx$ 200 R_E for magnetic field fluctuations. No previous study has considered the minimum and maximum of solar activity separately. Earlier single-spacecraft studies give values of correlation in Elsässer variables as $\lambda \approx 265\ R_E$ (Tu & Marsch 1995). More recent values correspond more closely to the values measured here; however all of these previous results are within error of the solar maximum correlation length of the magnetic field magnitude. See, for example, Goldstein et al. (1995) for further discussion of correlation lengths, and Matthaeus et al. (2008) for discussion of the difference between multispacecraft and single-spacecraft measurements of correlation.

Figure 4 shows the linear correlation measurements of the components of **B**. The points from solar maximum and minimum do not show any systematic difference for the $\hat{y}$ and $\hat{z}$ components, and only a slight systematic trend in the $\hat{x}$ component, unlike ρ and $|B|$ in Figure 3. Fitting an exponential function to the data, as before, yields the values of the correlation lengths for the components of **B** shown in Table 1. The B_y

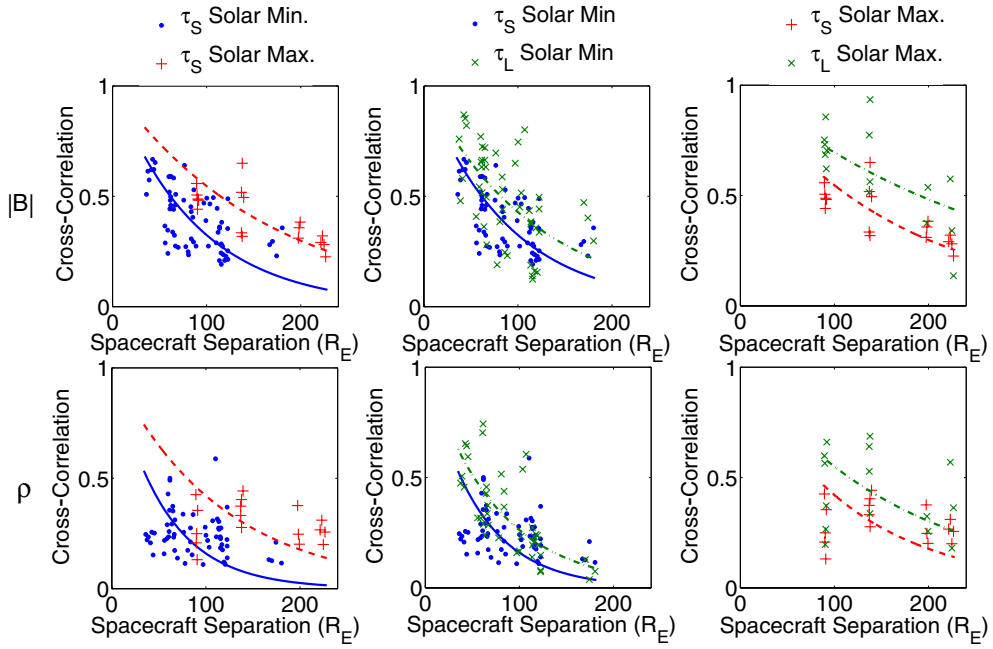

Figure 6. 24 hr mean linear correlation coefficients, calculated between *ACE* and *Wind* $|B|$ and ρ measurements. The shorter window τ_S is used at solar minimum (•) and solar maximum (+), and compared to the previous results using window τ_L (×) for both solar minimum and maximum. The solid lines are inverse exponential fits to the minimum data, and the dashed lines are inverse exponential fits to the maximum data.

(A color version of this figure is available in the online journal.)

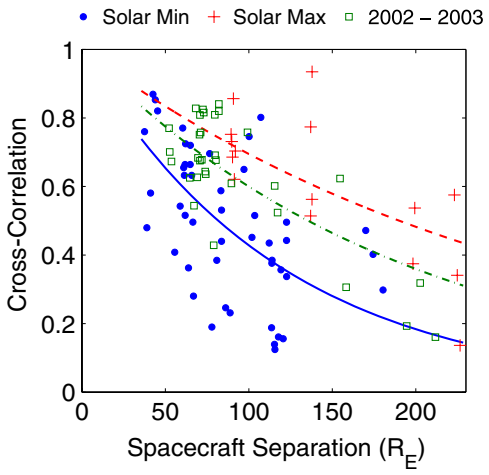

Figure 7. Cross-correlation measurements of $|B|$ midway through the solar cycle in 2002 and 2003 (green squares) superimposed on Figure 3, using window length τ_L. The fitted exponential decay (dot-dashed line) lies directly between those for solar minimum and solar maximum and has an intermediate correlation length λ of 195 R_E. The value of R^2 for this measurement is 0.6.

and B_z values of λ_{max} and λ_{min} are within uncertainty of each other, and are distinct from the values for $|B|$ and ρ. The estimated correlation lengths, λ, and the scatter on these values estimated using window τ_L discussed so far are summarized in Figure 5 and Table 1.

The uncertainties—some large—on these values arise primarily from the scatter of the measurements, presumably due to the highly variable nature of the solar wind. We discuss this in more depth below. However, for now we can conclude that the level of scatter nevertheless allows us to infer a systematic trend: $\lambda(|B|)_{min} > \lambda(\rho)_{min}$, $\lambda(|B|)_{min} < \lambda(|B|)_{max}$, and $\lambda(\rho)_{min} < \lambda(\rho)_{max}$. We can also infer that the correlation lengths of the $\hat{y}$ and $\hat{z}$ GSE components of **B** at solar maximum and minimum are indistinguishable within the scatter. The scatter in the estimated linear correlation of the $\hat{x}$ GSE component of **B** prevents meaningful estimation of its correlation length.

Figure 6 compares the measured linear correlation coefficient from the two different time windows, $\tau_L = 960$ minutes and $\tau_S = 200$ minutes. The shorter window more closely corresponds to the inertial range of solar wind turbulence; thus, it should minimize the effect of large-scale structures on the estimated correlation lengths. We find smaller values for the correlation length than for the longer time window, as tabulated in Table 1: $\lambda^{\tau_S}_{min}(|B|) = 89^{+8}_{-7} R_E$, $\lambda^{\tau_S}_{min}(\rho) = 55^{+7}_{-6} R_E$. This difference is more marked at solar maximum where the correlation lengths measured by the shorter window are considerably smaller than in Table 1: $\lambda^{\tau_S}_{max}(|B|) = 166^{+26}_{-21} R_E$ and $\lambda^{\tau_S}_{max}(\rho) = 116^{+35}_{-22} R_E$.

Overall, the shorter time window does not change the relative ordering of the correlation length scales between solar maximum and minimum, or between ρ and $|B|$, that we have identified with the longer window. Furthermore, these figures still suggest significant correlation for fluctuations on spatiotemporal scales within the inertial range of turbulence in the solar wind. We conclude that the solar cycle variation persists for τ_S within the inertial range.

As a final check that the solar cycle is the main factor affecting the changing correlation lengths of $|B|$ and of ρ, a period of data from 2002 and 2003 is used to investigate the declining phase of the solar cycle. For approximately 6 months from 2002 December to 2003 May, both *ACE* and *Wind* orbited the L1 point and provided similar observations to those used earlier for solar minimum. The measured correlation length of $|B|$ over 32 days from this period is $\lambda(|B|) = 195^{+34}_{-25} R_E$ with an R^2 value of 0.6: see Figure 7. This measurement lies directly between the values at solar minimum and maximum, lending further support to the

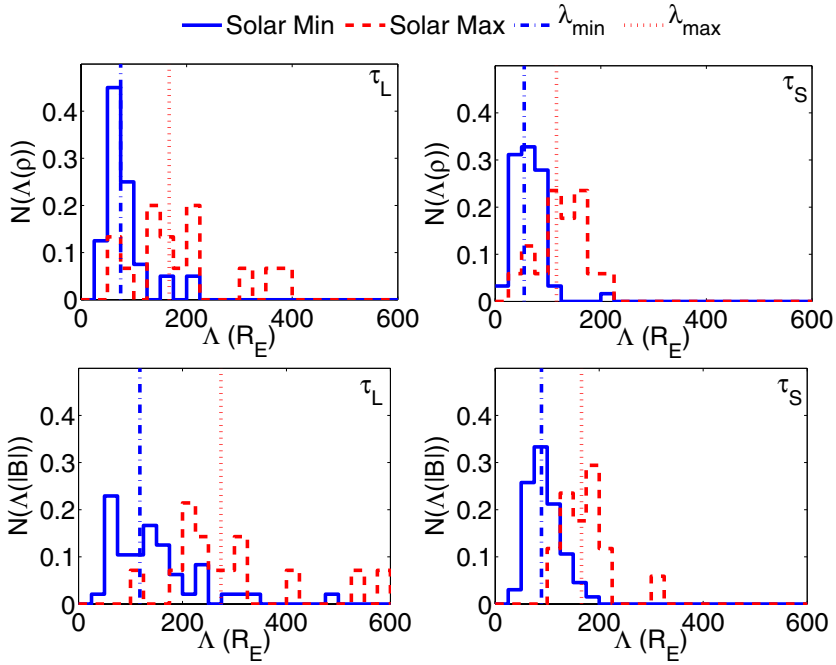

Figure 8. Frequency–magnitude histogram for distributions of fitted linear correlation lengths Λ between *ACE* and *Wind*, inferred from data using Equations (3) and (4), for $|B|$ (bottom panels) and ρ (top panels) using windows τ_S (right panels) and τ_L (left panels). Histograms at solar minimum are shown as blue bars, and at maximum as red bars. The correlation lengths in Table 1 are shown as vertical dashed lines for minimum and dot-dashed lines for maximum. The histograms are normalized such that the area under the bars is equal to 1 at both maximum and minimum.

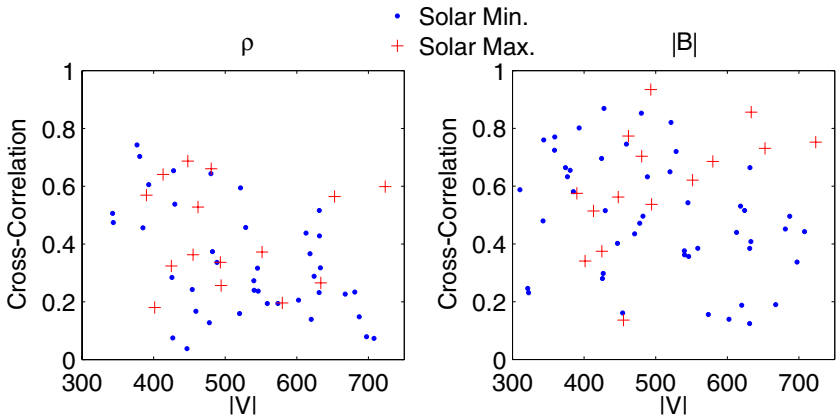

Figure 9. Linear correlation of $|B|$ observed by *ACE* and *Wind* plotted against mean solar wind velocity using window τ_L. Solar minimum (•) and solar maximum (+). No clear trend is present in the data.

(A color version of this figure is available in the online journal.)

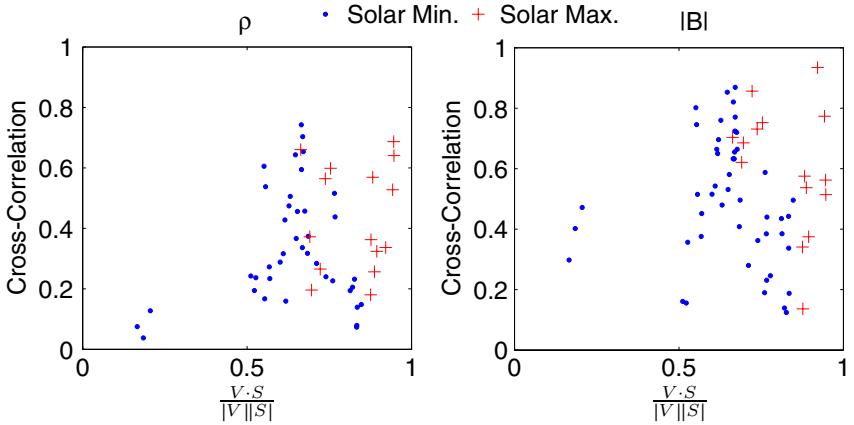

Figure 10. Linear correlation of $|B|$ observed by *ACE* and *Wind* plotted against mean spacecraft orientation as estimated by $(V \cdot S)/|V||S|$ where V is the solar wind velocity and S the spacecraft separation vector using window τ_L. Solar minimum (•) and solar maximum (+). No clear trend is present in the data.

(A color version of this figure is available in the online journal.)

argument that solar activity changes the correlation length of the magnitude of the magnetic field.

We now look in more detail at the large amount of scatter in the above plots. Figure 8 shows the correlation lengths estimated from individual linear correlation coefficient with window τ_L. This is done by inverting the exponential to estimate individual values of the correlation length Λ for each measurement of correlation coefficient:

$$C = e^{-S/\Lambda} \tag{3}$$

$$\Lambda = \frac{-S}{\ln(C)}, \tag{4}$$

where Λ is the estimated correlation length, S is the spacecraft separation length, and C is the measured linear correlation coefficient for each variable (ρ, $|B|$, B_x, B_y, B_z). Histograms for the value of Λ at maximum and minimum for $|B|$ and ρ are plotted in Figure 8 with bin widths of 50 R_E for both values of τ. Although the histograms overlap slightly, the peak values in the histograms at minimum are consistently lower than the peaks at maximum, by at least one bin width, for both variables and both time windows. This makes them clearly distinguishable as separate peaks. Figure 8 thus provides a strong indication that the distribution of correlation lengths measured at maximum is different from that at minimum for both $|B|$ and ρ.

In Figures 9 and 10, we explore whether solar wind speed and the orientation of the vector separation of the pair of spacecraft with respect to the solar wind flow direction contribute to the secular variation with solar cycle or to the scatter found in the estimated values of linear correlation. Figure 9 plots cross-correlation against solar wind speed for both ρ and $|B|$. The full range of expected solar wind speed values ($\approx$ 300–700 km s^{-1}) is covered by the set of observations, and there is no apparent trend with solar wind speed in the level of linear correlation between the two spacecraft. The scatter is thus not straightforwardly a result of changing conditions due to variation in solar wind speed.

Figure 10 shows the effect of spacecraft orientation on the linear correlation coefficient measured. Spacecraft orientation is measured by calculating the scalar product of the vector separation $\mathbf{S}$ of the spacecraft with the measured solar wind velocity $\mathbf{V}$, normalized by the separation and solar wind speed: $(\mathbf{V} \cdot \mathbf{S})/(|V||S|)$. There is a systematic effect separating the solar maximum and minimum data, due to the different spacecraft orbits during maximum and minimum. However, we see that the correlation coefficients are not ordered with the spacecraft orientation; instead there is a broad scatter in the levels of linear correlation for the different values of spacecraft orientation, which completely overlap for solar maximum and minimum.

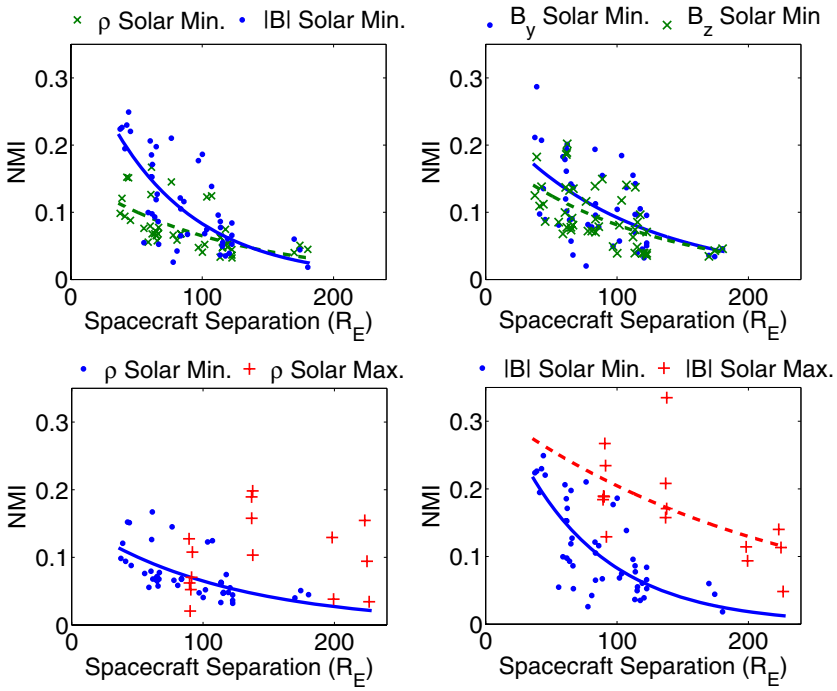

Figure 11. NMI calculated between *ACE* and *Wind* observations of $|B|$, ρ, and the $\hat{y}$ and $\hat{z}$ GSE components of **B**, plotted against spacecraft separation. Window τ_L was used in all cases. Solar minimum (•) and solar maximum (+). The lines are decaying exponentials fitted to help guide the eye. No fit is shown for the ρ results at maximum as the scatter of the results prevents an accurate fit.

(A color version of this figure is available in the online journal.)

Thus while the spacecraft orientation changes during the solar cycle, this does not affect the range of correlations measured and cannot account for the trends seen in the previous figures.

4. MUTUAL INFORMATION

We use MI (Johnson et al. 2005; Shannon 1948; March et al. 2005; Sello 2001; Wicks et al. 2007) to provide a nonlinear measure of the correlation in the data. This enables us to check the linear correlation results using an independent technique and thus verify the salient trends shown above. MI quantifies the information content shared by two signals A and B. For discrete signals we can write the MI as

$$I(A, B) = \sum_{i,j}^{m} P(a_i, b_j) \log_2 \left(\frac{P(a_i, b_j)}{P(a_i)P(b_j)} \right). \quad (5)$$

Here, the signals A and B have been partitioned into an alphabet (a discrete set which spans the possible values the signal can take) so that $A = \{a_1, \ldots, a_i, \ldots, a_m\}$ where a_1 and a_m are the extrema of A found in all data considered. The discretized signal takes value a_i with probability $P(a_i)$ and similarly for b_i we have $P(b_i)$, while $P(a_i, b_j)$ is the joint probability of a_i and b_j. The chosen base of the logarithm defines the units in which the MI is measured. Normally base 2 is used, so that the MI is measured in bits. If one defines the entropy of a signal as

$$H(A) = -\sum_{i}^{m} P(a_i) \log_2(P(a_i)), \quad (6)$$

then MI can be written as a combination of entropies (Shannon 1948)

$$I(A, B) = H(A) + H(B) - H(A, B). \quad (7)$$

The calculation of the entropies needed to form the MI is not trivial, as there is some freedom in the method of discretization of the signals and in the method used to estimate the probabilities $P(a_i)$, $P(b_j)$, and $P(a_i, b_j)$. There are many different methods currently used, summarized and compared by Cellucci et al. (2005) and Kraskov et al. (2004). For spacecraft observations of the solar wind, we use a discretization based on the standard deviation σ of the data. Only data within 5σ of the mean are considered and bins of width $\sigma/2$ are used, giving 20 bins in total. The form of MI used here is the normalized mutual information (NMI; Studholme et al. 1999), which is $I(A, B)$ normalized by the joint entropy $H(A, B)$ so as to remove the dependence on the entropy of the solar wind at the time of observation:

$$\mathrm{NMI}(A, B) = \frac{H(A) + H(B)}{H(A, B)} - 1. \quad (8)$$

This gives results in the range $0 \leqslant \mathrm{NMI} \leqslant 1$ facilitating direct comparison between different periods of data.

We have repeated the analysis described above but calculating the NMI in each time window, τ_S and τ_L, instead of the cross-correlation. Some example results are shown in Figure 11. The results shown above using linear cross-correlation are confirmed by the NMI. The NMI measured between spacecraft observations of ρ is lower than that of $|B|$ and the components of **B**. The NMI measured at solar maximum is higher than that at solar minimum for $|B|$ and ρ, although we are unable to quantify this in the same way as for cross-correlation because we do not a priori have the functional dependence of NMI on distance in a turbulent plasma. An exponential function $y = a \exp(-S/\xi)$ provides a simple local parameterization of the NMI results;

however in order to fit the data satisfactorily both a and ξ must be allowed to vary and thus no MI correlation lengths can be estimated.

5. CONCLUSIONS

We have used simultaneous data from the *ACE* and *Wind* spacecraft separated by between 30 R_E and 220 R_E, to calculate the spatial correlation lengths of upstream solar wind ρ, $|B|$, and **B** components. At solar minimum we have 48 days of contemporaneous *Wind* and *ACE* observations. Several trends can be seen by eye in plots of linear versus spacecraft separation, and we quantify these by fitting exponentials. We also estimate the uncertainty due to the scatter in the data using a nonlinear least-squares fit. We determine the linear correlation length scale of ρ to be $\lambda(\rho) \approx 75^{+11}_{-9} R_E$. This is measurably smaller than $\lambda(|B|) \approx 118^{+21}_{-15} R_E$.

At solar maximum we have 15 days of contemporaneous *Wind* and *ACE* data. This allows us to investigate the effect of the solar cycle. We find that although there is a large scatter in all measured correlations, $\lambda(|B|)$ and $\lambda(\rho)$ at solar maximum are larger than at minimum by a factor of 2. In contrast, the components of the magnetic field show weak variation with solar cycle. We have used two window lengths: one that emphasizes the inertial range of turbulence seen in the solar wind (200 minutes), and the other on longer timescales (960 minutes). The window on inertial range timescales gives values of λ that are systematically shorter than, but within the uncertainties of, the values obtained from the longer window.

The scatter on these data is investigated by creating histograms of the individual linear correlation lengths estimated from the data. The peaks in these distributions for solar maximum and minimum are clearly distinguishable for both window lengths τ_S and τ_L. We thus conclude that the solar cycle dependence of the correlation length is independent of our chosen window sizes.

The scatter in the results is presumably due to variability in solar wind conditions. We found no clear ordering of the data with respect to solar wind speed or the relative orientation of the pair of spacecraft. Hence selecting or rejecting data using criteria based on these parameters does not reduce the observed scatter in the observations.

NMI is used as a complementary nonlinear measure of correlation. NMI measurements give the normalized Shannon information shared between the spacecraft to be lower for ρ than for $|B|$, which is consistent with the results using linear correlation. However, the dependence of NMI on distance is not known for turbulent media; we thus fit the NMI results with an exponential to give a local estimate of correlation length but cannot calculate values of λ for these results.

An intriguing aspect of these results is that the correlation lengths of both ρ and $|B|$ increase by a factor of approximately 2 from solar minimum to solar maximum. The components of the magnetic field are, to the precision that this methodology allows, insensitive to the solar cycle. This behavior persists when we restrict our analysis to timescales within that identified as the inertial range of turbulence in the solar wind, as well as on longer temporal scales. These phenomena invite interpretation in terms of the relative role of coronal driving and subsequent in situ evolution, particularly through Alfvénic nonlinearity and turbulence. Our analysis of the observations then suggests a scenario in which the magnetic field components are dominated by solar wind evolution in situ, and are thus insensitive to changes in the solar corona whereas the spatial correlation of the field magnitude and the density are dominated by coronal structure and dynamics, and accordingly reflect changes in coronal complexity with the solar cycle.

This interpretation is consistent with recent single-spacecraft results (Kiyani et al. 2007; Hnat et al. 2007) which show solar cycle dependence within the inertial range of magnetic energy density fluctuations, and with results from the quiet fast solar wind that show that the magnetic field components in the inertial range are insensitive to spacecraft location with respect to the corona (Nicol et al. 2008). Our results provide an estimate of the change in correlation length of ρ and **B** in the solar wind over the solar cycle which can be included in models of cosmic ray propagation. One can go further and speculate that the fact that ρ and $|B|$ correlation length scales show the same degree of modulation by a factor of 2 with the solar cycle suggests that both these parameters are affected by the same aspects of coronal structure and dynamics that have solar cycle dependence.

The fact that the correlation lengths of ρ and $|B|$ differ in magnitude, while tracking each other at the minimum and maximum of the solar cycle, may be due to the initial conditions in the corona if the solar wind has not had adequate time to completely equilibrate via turbulent processes in its flight from the Sun to the Earth. The difference in the correlation length scale between $|B|$ and the field components may simply reflect the fact that these capture different physical processes: for example, compressive versus shear Alfvénic fluctuations or, at larger temporal scales, different aspects of propagating coherent structures of coronal origin. These correlation lengths need not be the same.

Finally, we find that the correlation lengths of ρ, B_y, and B_z are very similar at solar maximum, at least to the precision of the methodology used here. The estimate of the ρ correlation length that we obtain is less accurate than that of B_y and B_z, so this outcome may be coincidental, but it warrants further investigation.

The authors acknowledge the STFC, EPSRC, and UKAEA for support; the CSC (Warwick) for computing facilities; and the *Wind* MFI and SWE teams and the *ACE* MAG and SWEPAM teams for data provision.

REFERENCES

Bame, S. J., Asbridge, J. R., Feldman, W. C., & Gosling, J. T. 1976, ApJ, 207, 977
Bruno, R., Bavassano, B., D'Amicis, R., Carbone, V., Sorriso-Valvo, L., & Pietropaolo, E. 2006, Space Sci. Rev., 122, 321
Cellucci, C. J., Albano, A. M., & Rapp, P. E. 2005, Phys. Rev. E, 71, 066208
Goldstein, M. L., Roberts, D. A., & Matthaeus, W. H. 1995, ARA&A, 33, 283
Hapgood, M. A. 1992, Planet. Space Sci., 40, 5, 711
Hapgood, M. A., Lockwood, M., Bowe, G. A., Willis, D. M., & Tulunay, Y. K. 1991, Planet. Space Sci., 39, 3, 411
Hill, M. E., Hamilton, D. C., & Krimigis, S. M. 2002, ApJ, 572, L169
Hnat, B., Chapman, S. C., Kiyani, K., Rowlands, G., & Watkins, N. W. 2007, Geophys. Res. Lett., 34, L15108
Johnson, J. R., & Wing, S. 2005, J. Geophys. Res., 110, A04211
Kiyani, K., Chapman, S. C., Hnat, B., & Nicol, R. M. 2007, Phys. Rev. Lett., 98, 211101
Kraskov, A., Stögbauer, H., & Grassberger, P. 2004, Phys. Rev. E, 69, 066138
March, T. K., Chapman, S. C., & Dendy, R. O. 2005, Geophys. Res. Lett., 32, L04101
Mason, G. M., et al. 2008, ApJ, 678, 1458
Matthaeus, W. H., Dasso, S., Weygand, J. M., Milano, L. J., Smith, C. W., & Kivelson, M. G. 2005, Phys. Rev. Lett., 95, 231101
Matthaeus, W. H., Weygand, J. M., Chuychai, P., Dasso, S., Smith, C. W., & Kivelson, M. G. 2008, ApJ, 678, L141

Milano, L. J., Dasso, S., Matthaeus, W. H., & Smith, C. W. 2004, Phys. Rev. Lett., 93, 155005
Moore, D. S., & McCabe, G. P. 2006, Introduction to the Practice of Statistics 5th ed. (New York, NY: Freeman)
Nicol, R. M., Chapman, S. C., & Dendy, R. O. 2008, ApJ, 679, 862
Osman, K. T., & Horbury, T. S. 2007, ApJ, 654, L103
Parhi, S., Bieber, J. W., Matthaeus, W. H., & Burger, R. A. 2002, Geophys. Res. Lett., 29, 1258
Pommois, P., Veltri, P., & Zimbardo, G. 2001, J. Geophys. Res., 106, 24965
Qin, G., Matthaeus, W. H., & Bieber, J. W. 2006, ApJ, 640, L103
Ridley, A. J. 2000, J. Atmos. Sol.-Terr. Phys., 62, 757
Ruffolo, D., Matthaeus, W. H., & Chuychai, P. 2003, ApJ, 597, L169
Sello, S. 2001, A&A, 377, 312
Shannon, C. E. 1948, Bell Syst. Tech. J., 27, 379
Studholme, C., Hill, D. L. G., & Hawkes, D. J. 1999, Pattern Recognit., 32, 71
Taylor, G. I. 1938, Proc. R. Soc., A164, 476
Tu, C.-Y., & Marsch, E. 1995, Space Sci. Rev., 73, 1
Webber, W. R., McDonald, F. B., & Lukasiak, A. 2003, ApJ, 599, 582
Weimer, D. R., Ober, D. M., Maynard, N. C., Collier, M. R., McComas, D. J., Ness, N. F., Smith, C. W., & Watermann, J. 2003, J. Geophys. Res., 108, 1026
Wicks, R. T., Chapman, S. C., & Dendy, R. O. 2007, Phys. Rev. E, 75, 051125
Zank, G. P., Matthaeus, W. H., Bieber, J. W., & Moraal, H. 1998, J. Geophys. Res., 103, 2085